

Security-Robustness Trade-offs in Diffusion Steganography: A Comparative Analysis of Pixel-Space and VAE-Based Architectures

Yuhua Xu¹, Wei Sun¹, Chengpei Tang¹, Jiaying Lu¹, Jingying Zhou¹, Chen Gu¹

Abstract—Current generative steganography research mainly pursues computationally expensive mappings to perfect Gaussian priors within single diffusion model architectures. This work introduces an efficient framework based on approximate Gaussian mapping governed by a scale factor calibrated through capacity-aware adaptive optimization. Using this framework as a unified analytical tool, systematic comparative analysis of steganography in pixel-space models versus VAE-based latent-space systems is conducted. The investigation reveals a pronounced architecture dependent security-robustness trade-off: pixel-space models achieve high security against steganalysis but exhibit fragility to channel distortions, while VAE-based systems like Stable Diffusion offer substantial robustness at the cost of security vulnerabilities. Further analysis indicates that the VAE component drives this behavior through opposing mechanisms where the encoder confers robustness via manifold regularization while the decoder introduces vulnerabilities by amplifying latent perturbations into detectable artifacts. These findings characterize the conflicting architectural roles in generative steganography and establish a foundation for future research.

Index Terms—Generative Steganography, Diffusion Models, Latent Diffusion Models, VAE, Security-Robustness Trade-off.

I. INTRODUCTION

THE rapid proliferation of generative artificial intelligence systems has substantially transformed the digital media landscape, with billions of synthetic images now generated daily through diffusion models [1], generative adversarial networks [2], and related architectures [3]. This abundance of AI-generated content creates a substantially different environment for covert communication, where synthetic media becomes commonplace rather than exceptional. In this context, steganography—the practice of concealing secret information within seemingly innocuous cover media—finds new opportunities [4]. Unlike encryption approaches that protect message content while revealing communication existence, steganography seeks to hide both the message and the communication act itself. The widespread presence of synthetic content thus provides

natural camouflage for such covert activities, offering plausible cover for artificially generated stego images.

Traditional steganography methods have followed two distinct paradigms for covert communication in digital media. Modification-based steganography evolved from early least significant bit (LSB) manipulation [5] to sophisticated adaptive embedding methods [6]–[9] based on syndrome-trellis codes (STC) [10] that minimize embedding distortion through optimal pixel selection. Despite considerable sophistication, these methods face a fundamental limitation: any modification to existing cover images inevitably leaves detectable traces exploitable by increasingly powerful deep learning-based steganalysis tools [11]–[14]. Selection-based steganography addresses these vulnerabilities by mapping secret information to image features and selecting appropriate cover images from large databases rather than modifying existing content [15]–[18]. However, these approaches require massive image repositories to reduce cover collision probability and suffer from inherently low embedding rates, limiting practical applicability for high-capacity covert communication scenarios.

The constraints of traditional paradigms have driven the advancement of Generative Image Steganography (GIS), which directly synthesizes stego images by integrating information embedding within the generative process. Diffusion models provide an advantageous framework for GIS implementation, given their inherent capability to transform standard Gaussian distribution (SGD) noise priors into high-fidelity image representations. This inherent capability has led the research community to focus primarily on a singular challenge: how to map a secret message into an initial noise vector that is statistically indistinguishable from the model’s SGD prior [19]–[22]. While this focus is well-motivated, it has inadvertently created two significant research gaps. Firstly, the pursuit of perfect statistical conformity has yielded a suite of increasingly complex and computationally expensive mapping functions, potentially creating an unnecessary barrier to practical application. Secondly and perhaps more critically, by treating the generative model as a black box that reliably maps noise to an image, prior work has often overlooked the profound impact of the model’s internal architecture. Most studies are confined to a single paradigm—either direct pixel-space models or Variational autoencoders (VAE) [23] based latent-space [24] systems like Stable Diffusion [25]—

Corresponding author: Wei Sun and Chengpei Tang.

Yuhua Xu, Wei Sun, Jiaying Lu, Jingying Zhou and Chen Gu are with the School of Electronics and Information Technology (School of Microelectronics), Sun Yat-Sen University, Guangzhou 510006, China. e-mail: sunwei@mail.sysu.edu.cn; {xuyh55, lujx63, zhoujy229, guch9}@mail2.sysu.edu.cn

Chengpei Tang is with the School of Advanced Manufacturing, Sun Yat-Sen University, Shenzhen 518107, China. e-mail: tchengp@mail.sysu.edu.cn

with limited comparative analysis. Consequently, fundamental questions regarding how architectural choices influence security, robustness, and their intrinsic trade-offs remain unexplored. This gap is particularly pressing given the diverse architectures of modern generative systems, whose internal mechanisms may introduce unique vulnerabilities or afford new opportunities for steganography.

To address these research gaps, we propose a steganography framework that enables systematic comparative analysis across different generative architectures. Our approach employs an efficient approximate Gaussian mapping with two primary objectives: reducing computational overhead relative to SGD mapping methods, and evaluating whether near Gaussian distributions can achieve comparable performance to perfect mappings across key metrics including security, robustness, and embedding capacity. Should performance prove comparable, this would indicate that perfect statistical conformity may not be essential, thereby expanding the design space for alternative mapping strategies. This framework facilitates cross-architectural comparisons that have remained largely unexplored in prior work despite their technical feasibility. Serving as a unified analytical tool, it enables the first systematic comparative study of steganography performance in pixel-space diffusion models versus VAE-based latent-space systems. Experimental results reveal evidence of a notable trade-off between security and robustness that appears to be associated with the underlying architecture. The primary contributions can be summarized as follows:

- This work introduces a steganography framework based on computationally efficient approximate Gaussian mapping and adaptive optimization. The framework demonstrates that SGD may not be necessary for effective steganography, while enabling systematic cross-architectural analysis.
- A comparative analysis provides evidence for an architecture dependent security-robustness trade-off. Experimental results indicate that pixel-space models can achieve higher security levels but exhibit greater fragility, while VAE-based systems offer enhanced robustness while introducing detectable artifacts.
- A mechanistic analysis examines the VAE's role in this trade-off. The investigation reveals that the encoder contributes to robustness through manifold projection of distorted inputs, while the decoder may amplify subtle latent perturbations into pixel-space artifacts detectable by steganalysis tools.

The remainder of this paper is organized as follows. Section II reviews pertinent prior research. Section IV elaborates on our framework, including the noise mapping, data hiding and extraction processes, and the adaptive optimization strategy. Section V details the experimental configuration, evaluation metrics, and presents a comprehensive analysis of the empirical results. Finally, Section VI summarizes our findings and outlines future research directions.

II. RELATED WORKS

The evolution of image steganography has been characterized by a continuous pursuit of higher embedding capacity, improved

imperceptibility, and greater resilience against steganalysis. This pursuit has driven the field through several distinct paradigms, from methods that modify existing cover images to approaches that synthesize stego images directly from secret messages.

A. Modification and Selection-Based Steganography

Traditional steganography involves introducing subtle alterations to a cover image to embed secret information. Early techniques such as Least Significant Bit (LSB) replacement [5] and its matching variants [26] were computationally simple but produced predictable statistical artifacts, making them detectable by basic analysis methods [27]. This limitation led to the development of adaptive steganography, where embedding modifications are concentrated in image regions of high complexity, such as textured areas, where they are less likely to disrupt the cover's natural statistics.

The core innovation in this domain was the design of distortion functions that assign modification costs to cover elements, enabling secret message embedding while minimizing total distortion. Syndrome-Trellis Codes (STC) [10] provided the practical implementation framework by separating coding from distortion design, allowing researchers to focus on developing refined cost functions across different domains. Consequently, STC became the backbone for a generation of adaptive methods, including HUGO [6], S-UNIWARD [7], HILL [8] and WOW [9], each proposing novel ways to define embedding costs. However, the modification process remains a potential vulnerability. The development of deep learning-based steganalysis methods, such as SRNet [11], XuNet [12], YeNet [13], and SiastegNet [14], has demonstrated substantial capability to detect the subtle and high-dimensional signatures produced by advanced embedding algorithms.

To address modification-related vulnerabilities, selection-based steganography emerged as an alternative paradigm. These methods establish mappings between unmodified image features and secret messages, then select images from large databases that satisfy these mappings [15]–[18]. While theoretically immune to steganalysis techniques that target embedding artifacts, selection-based methods are constrained by two practical challenges. Firstly, they require maintaining a massive and diverse image repository to ensure a high probability of finding a suitable cover for any given message. Secondly, they are characterized by low embedding capacities, rendering them impractical for applications requiring substantial data transmission. The constraints of both traditional paradigms have motivated the exploration of generative approaches that can potentially address these fundamental limitations.

B. Generative Image Steganography

Generative Image Steganography (GIS) synthesizes stego images directly from secret information, seeking to combine the security benefits of selection-based approaches with the embedding capacity of modification-based methods. The GIS process involves two core stages: mapping secret messages into SGD noise, and utilizing pre-trained generative models to synthesize stego images. The choice of generative architecture

and the design of the message-to-noise mapping function determine the characteristics of a GIS system.

Early GIS explorations primarily employed Generative Adversarial Networks (GANs), which spawned diverse integration strategies. Initial approaches used GANs solely to synthesize realistic cover images, into which messages were subsequently embedded using conventional modification techniques [28], [29]. More sophisticated methods sought to embed secret data directly within the generative process by mapping messages to SGD noise in the GAN’s latent space and using the generator to produce stego images. These methods varied in their embedding strategies: some mapped secrets to semantic attributes such as image categories [30], while others incorporated structural or textural information derived from the secret [31]. Notable recent works by Wei et al. [32] and Su et al. [33] adapted StyleGAN2 by directly modulating intermediate feature maps with secret data. Specifically, Su et al. developed a distribution preserving method that leverages the symmetric properties of Gaussian distributions to embed binary secrets while preserving statistical validity. However, GAN-based steganography faces fundamental architectural limitations. The primary challenge stems from the non-invertible nature of most GAN generators, which precludes straightforward analytical reversal from generated images to latent codes. This necessitates training separate extractor networks [34], creating a two-part optimization process that often results in trade-offs between message retrieval accuracy and stego image quality.

While invertible generative models such as Glow [3] have also been explored for steganography purposes [22], diffusion models have emerged as the dominant paradigm for contemporary GIS. This preference stems not solely from their theoretical invertibility, but from several advantageous properties. Diffusion models can be formulated using ordinary differential equations (ODEs) [35], enabling the application of efficient numerical solvers [36], [37] that generate high-quality images with significantly fewer iterative steps compared to the original sampling procedures. Within this paradigm, steganography is formulated as the reverse of the model’s forward noising process, where secret-infused Gaussian noise vectors serve as initial states \mathbf{x}_T .

Within generative steganography paradigms such as GANs, diffusion models, and invertible models like Glow, the fundamental research challenge centers on effectively encoding secret information into SGD noise. This transformation process represents the core technical bottleneck that determines both the security and capacity characteristics of any GIS system, regardless of the underlying generative architecture. The universal nature of this challenge stems from the fact that most generative models are designed to operate with Gaussian priors, necessitating the transformation of arbitrary secret data into statistically valid noise representations.

Within the diffusion-based GIS framework, this fundamental mapping challenge has given rise to two distinct research paradigms, each addressing different application scenarios and performance priorities. The first paradigm pursues lossless recovery of secret information, aiming to achieve 100% accuracy in retrieving the original secret data. The central research challenge involves designing mapping functions that

transform secret messages into SGD noise vectors that are both perfectly invertible for bit-level recovery and statistically indistinguishable from the model’s prior distribution $\mathcal{N}(\mathbf{0}, \mathbf{I})$. Researchers have developed various mapping strategies, including probability integral transform [19], central limit theorem applications [20], inverse discrete cosine transform properties [21], and positional encoding of pre-sampled SGD noise [22]¹. While theoretically elegant, these methods often incur computational overhead due to the stringent requirement of perfect statistical matching and may exhibit capacity limitations.

The second paradigm recognizes that certain types of secret data, particularly images, contain substantial redundancy that renders perfect bit-level recovery unnecessary. Instead of pursuing lossless reconstruction, these methods prioritize perceptual fidelity, where the recovered secret need only be visually indistinguishable from the original. This relaxed requirement enables significantly higher embedding rates. Yu et al. [38] demonstrated this approach by leveraging diffusion models’ inherent capability to transform secret images into noise-like Gaussian representations through the forward noising process. Chen et al. [39] enhanced this framework by employing complex distribution-preserving mapping mechanisms to achieve secret information to SGD conversion, further improving recovered secret image quality through order-preserving codebooks. These methods achieve high effective bitrates (up to 24 bpp) by exploiting perceptual redundancy and are evaluated using image quality metrics (PSNR/SSIM) rather than bit-level retrieval accuracy.

III. PRELIMINARIES

This section establishes the technical foundations of diffusion models, focusing on the evolution from stochastic formulations to deterministic ODE-based frameworks and the development of efficient numerical solvers that enable invertible transformations for steganography applications.

A. From Stochastic Processes to Deterministic ODE Flow

The denoising diffusion probabilistic model (DDPM) [1] defines a discrete-time forward Markov chain that adds Gaussian noise over T steps according to a variance schedule $\{\beta_t\}_{t=1}^T$. Any noisy state \mathbf{x}_t can be expressed directly in terms of the initial data \mathbf{x}_0 and a Gaussian noise sample ϵ :

$$q(\mathbf{x}_t|\mathbf{x}_0) = \mathcal{N}(\mathbf{x}_t; \sqrt{\bar{\alpha}_t}\mathbf{x}_0, (1 - \bar{\alpha}_t)\mathbf{I}), \quad (1)$$

where $\alpha_t = 1 - \beta_t$ and $\bar{\alpha}_t = \prod_{i=1}^t \alpha_i$. The reverse process is parameterized by a neural network $\epsilon_\theta(\mathbf{x}_t, t)$, typically implemented as an attention-based U-Net architecture, trained to predict the noise component ϵ from the noisy input \mathbf{x}_t .

While effective for generation tasks, the stochastic nature of the original DDPM formulation prevents deterministic message retrieval, limiting early diffusion-based steganography approaches. A more suitable foundation emerges from the continuous-time generalization described by a stochastic differential equation (SDE). For any such SDE, there exists an

¹Note that [22] employs the invertible Glow model rather than diffusion models for image generation, demonstrating that the core mapping challenge transcends specific generative architectures.

associated deterministic process, known as the probability flow ODE [35], that shares the same marginal probability densities $p_t(\mathbf{x})$:

$$d\mathbf{x} = \left[\mathbf{f}(\mathbf{x}, t) - \frac{1}{2}g^2(t)\nabla_{\mathbf{x}} \log p_t(\mathbf{x}) \right] dt. \quad (2)$$

Here, $\mathbf{f}(\cdot, \cdot)$ represents the drift function, $g(\cdot)$ denotes the diffusion coefficient, and the score function $\nabla_{\mathbf{x}} \log p_t(\mathbf{x})$ is approximated using the trained denoiser ϵ_{θ} . This ODE defines a deterministic mapping between the noise domain at time T_{max} and the data domain at time 0. The theoretical invertibility of this ODE provides the foundation for reliable message recovery, enabling widespread adoption of diffusion models in steganography research. A secret message encoded as initial noise $\mathbf{x}_{T_{max}}$ can be recovered from the generated image \mathbf{x}_0 by integrating the ODE in reverse.

B. Efficient Integration via Advanced ODE Solvers

The practical utility of the probability flow ODE in Eq. (2) for steganography hinges on solving it both efficiently and accurately. Direct numerical integration is computationally prohibitive, which motivated the development of specialized solvers. Early progress was made by denoising diffusion implicit model (DDIM) [40], which provided a first-order discretization that significantly accelerated sampling.

To achieve higher accuracy with even fewer steps, high-order solvers like DPM-Solver [36] were developed. These methods are particularly effective because they reformulate the ODE for numerical stability. For instance, DPM-Solver introduces the noise schedule function $\lambda_t = \log(\alpha_t/\sigma_t)$, where α_t and $\sigma_t = \sqrt{1 - \bar{\alpha}_t}$ are the signal and noise schedule coefficients defined in Eq. (1), and defines:

$$\tilde{\epsilon}_{\theta}(\mathbf{x}_t, t) = \frac{\epsilon_{\theta}(\mathbf{x}_t, t) - \sigma_t \mathbf{x}_t}{\alpha_t}. \quad (3)$$

This transforms the ODE into a numerically stable form:

$$\frac{d\mathbf{x}}{d\lambda} = \alpha_t \tilde{\epsilon}_{\theta}(\mathbf{x}_t, t). \quad (4)$$

DPM-Solver applies multi-step methods to solve this reformulated ODE efficiently but exhibits numerical instability with large timesteps or high-order approximations. DPM-Solver++ [37] addresses these stability issues through a refined predictor-corrector scheme. For a k -step solver, the prediction step uses polynomial extrapolation:

$$\mathbf{x}_{n+1}^{(k)} = \frac{\alpha_{n+1}}{\alpha_n} \mathbf{x}_n + \alpha_{n+1} \sum_{j=0}^{k-1} c_j^{(k)} \tilde{\epsilon}_{\theta}(\mathbf{x}_{n-j}, t_{n-j}). \quad (5)$$

The corrector step refines this estimate:

$$\mathbf{x}_{n+1} = \frac{\alpha_{n+1}}{\alpha_n} \mathbf{x}_n + \alpha_{n+1} \sum_{j=0}^{k-1} d_j^{(k)} \tilde{\epsilon}_{\theta}(\mathbf{x}_{n+1-j}^{(k)}, t_{n+1-j}). \quad (6)$$

This high-order integration approach generates images of a quality surpassing that of earlier DDPM and DDIM samplers in as few as 10-20 function evaluations, a substantial acceleration over the hundreds or thousands of steps those methods require. By improving both sample fidelity and numerical stability,

this method offers a compelling combination of deterministic output, high generation quality, and computational efficiency. These properties make advanced solvers like DPM-Solver++ particularly suitable for steganographic applications, which demand reliable message extraction and practical generation speeds.

IV. PROPOSED METHOD

This section presents a generative steganography framework designed to enable systematic comparative analysis across different diffusion model architectures. Our approach employs an approximate Gaussian mapping governed by a single scale parameter S , which is optimized through an adaptive procedure that balances message retrieval accuracy against statistical security. The framework supports both pixel-space and VAE-based latent-space diffusion models, facilitating direct architectural comparison under controlled experimental conditions. An overview of the framework is illustrated in Fig. (1).

A. Secret Message Hiding and Extraction Process

Our framework leverages the deterministic and invertible nature of the Eq.(2) through numerical integration. The entire steganography process operates through carefully constructed initial noise vectors \mathbf{x}_T that encode secret messages.

To embed a secret message bitstream, it is first decomposed into a sequence of Q -bit integers m , where $m \in \{0, 1, \dots, 2^Q - 1\}$. Each integer m is mapped to a component of the initial noise vector \mathbf{x}_T via our proposed approximate Gaussian mapping, shown as Eq. (7) and Eq. (8). This mapping function, which will be discussed in the subsequent section, is governed by a scale factor S and an auxiliary noise seed K_N . The resultant vector \mathbf{x}_T is designed to approximate a standard Gaussian distribution. This vector serves as the initial state for the reverse diffusion process. The final stego image, \mathbf{x}_{stego} , is synthesized by numerically integrating the probability flow ODE backward in time from $t = T$ to $t = 0$, using an efficient ODE solver DPM-Solver++ [37].

An authorized receiver, in possession of the stego image \mathbf{x}_{stego} and the shared parameters (Q, S, K_N) , can recover the secret message. The extraction process inverts the generation:

- **Latent Inversion:** The stego image \mathbf{x}_{stego} is treated as the initial state \mathbf{x}_0 . The ODE is integrated forward in time from $t = 0$ to $t = T$, yielding an estimate of the original secret-infused noise vector $\hat{\mathbf{x}}_T$.
- **Message Demapping:** The receiver regenerates the auxiliary Gaussian noise using the shared seed K_N and subtracts it from the recovered vector $\hat{\mathbf{x}}_T$. The resulting signal is rescaled and quantized to recover an estimate of the original message integers \hat{m} through Eq. (9).

The scale factor S critically influences image quality, security, robustness, and message recovery accuracy, motivating the adaptive optimization procedure in Section IV-C.

B. Approximate Gaussian Mapping

Our framework employs a computationally efficient linear transformation that balances embedding performance with

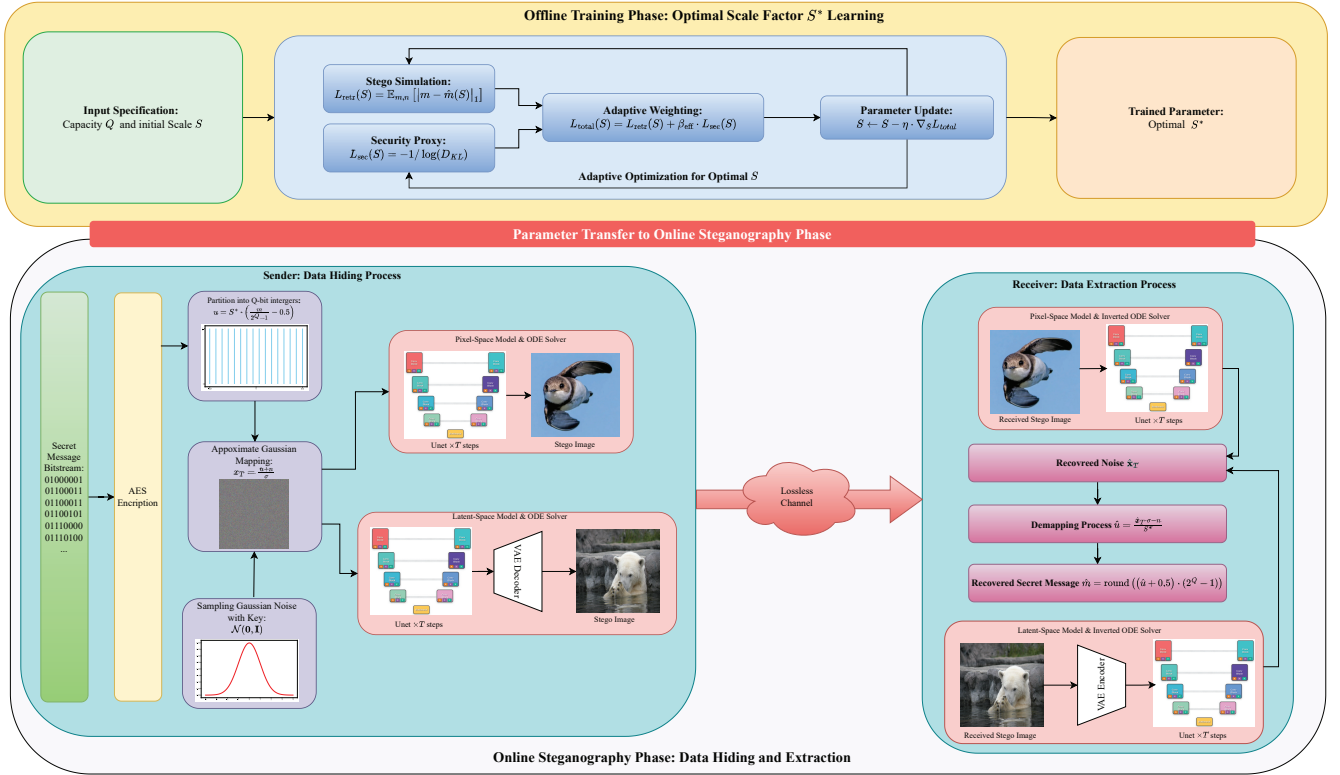


Fig. 1. Overview of the proposed steganography framework. The process consists of two phases. **Top, Offline Phase:** An adaptive optimization protocol learns the optimal scale factor S^* for a given capacity Q by balancing a retrieval loss L_{retr} with a KL-divergence-based security proxy L_{sec} . **Bottom, Online Phase:** The pre-computed S^* is used to map a secret message to an approximately Gaussian noise vector \mathbf{x}_T , which seeds a diffusion model (pixel-space or latent-space) to generate the stego image. The receiver inverts this deterministic process to extract the message.

practical implementation constraints. The approach processes secret messages partitioned into Q -bit integers, where each integer m is assumed to follow a discrete uniform distribution over $\{0, 1, \dots, 2^Q - 1\}$. This assumption is satisfied in practice through standard encryption techniques such as AES [41], which produce outputs that are computationally indistinguishable from random sequences.

The mapping process transforms each integer m into a noise component through a two-stage procedure. First, the integer is mapped to a zero-mean deterministic component:

$$u = S \cdot \left(\frac{m}{2^Q - 1} - 0.5 \right), \quad (7)$$

where S is the scale factor that controls the signal strength.

This deterministic signal is then combined with auxiliary Gaussian noise $n \sim \mathcal{N}(\mathbf{0}, \mathbf{I})$ generated using a shared secret key K_N . To ensure unit variance, the composite signal is normalized:

$$\mathbf{x}_T = \frac{u + n}{\sigma}, \quad \text{where } \sigma = \sqrt{1 + \text{Var}(u)}. \quad (8)$$

The variance of the message component u is determined by the properties of the discrete uniform distribution, yielding $\text{Var}(u) = \frac{S^2(2^Q + 1)}{12(2^Q - 1)}$. The resulting distribution of \mathbf{x}_T approximates a standard Gaussian, with approximation accuracy improving as S decreases.

$$\hat{m} = \text{round} \left(\left(\frac{\hat{\mathbf{x}}_T \cdot \sigma - n}{S} + 0.5 \right) \cdot (2^Q - 1) \right). \quad (9)$$

The scale factor S represents a fundamental trade-off parameter in the framework. A larger S increases the Euclidean distance between mapped message values, enhancing retrieval robustness against numerical errors, but simultaneously increases the statistical deviation from a SGD prior. Conversely, a smaller S improves security at the cost of a reduced error margin for retrieval. The optimization of S for a given capacity Q is addressed through the adaptive procedure described in Section IV-C.

An obvious advantage of this simple linear design is that it permits an online embedding process with constant time complexity, $\mathcal{O}(1)$. With the optimal S^* and σ^* pre-computed offline, the mapping operation is reduced to $\mathbf{x}_T = \text{LUT}[m] + C$, where C is a constant derived from the shared key and the lookup table (LUT) stores the 2^Q pre-calculated message-dependent values. This reduction to a single memory access and one addition eliminates the embedding process as a computational bottleneck, a critical advantage over methods requiring complex online transformations.

C. Adaptive Optimization of the Scale Factor S

The selection of an optimal scale factor S^* for a given embedding capacity Q requires balancing competing objectives of message retrieval accuracy and steganography security. We formulate this as a gradient-based optimization problem that treats S as the sole trainable parameter while maintaining the pre-trained diffusion model ϵ_θ in a frozen state. The

Algorithm 1: Adaptive Optimization of the Scale Factor

Input : Capacity Q ; Pre-trained Model ϵ_θ ; Target Accuracy Acc_{target} for given Q ; Hyperparameters $\beta_{base}, \{\gamma_k\}, \delta_1$
Output : Optimized Scale Factor S^*

```

1 Initialize scale factor  $S$ ;
2 while not converged do
3   Sample message batch
    $\mathbf{m}_{orig} \sim \text{UniformDiscrete}(0, 2^Q - 1)$ ;
4   // Perform steganography round-trip
    $\mathbf{x}_T \leftarrow \text{Map}(\mathbf{m}_{orig}, S, K_N)$  //Eq. (7) & (8)
    $\mathbf{x}_0 \leftarrow \text{Generate}(\epsilon_\theta, \mathbf{x}_T)$  //Backward ODE
   integration  $\hat{\mathbf{x}}_T \leftarrow \text{Invert}(\epsilon_\theta, \mathbf{x}_0)$  //Forward ODE
   integration  $\hat{\mathbf{m}} \leftarrow \text{Demap}(\hat{\mathbf{x}}_T, S, K_N)$  // Eq. (9)
5   // Compute loss components and current accuracy
    $L_{retr} \leftarrow \mathbb{E}[|\mathbf{m}_{orig} - \hat{\mathbf{m}}|_1]$  // Eq. (11)
    $D_{KL} \leftarrow \text{ComputeAnalyticalKL}(S, Q)$  // Eq. (12)
    $L_{sec} \leftarrow -1/\log(D_{KL})$ 
    $Acc_{curr} \leftarrow \text{Accuracy}(\mathbf{m}_{orig}, \hat{\mathbf{m}})$ 
6   // Adaptively set weight and compute total loss
    $\beta_{eff} \leftarrow \text{AdaptWeight}(\dots, Acc_{curr}, Acc_{target})$ 
    $L_{total} \leftarrow L_{retr} + \beta_{eff} \cdot L_{sec}$  //Eq. (10)
    $S \leftarrow S - \eta \cdot \nabla_S L_{total}$ 
7 end
8 return  $S^* \leftarrow S$ 

```

optimization minimizes a composite loss function that combines retrieval fidelity and statistical security:

$$L_{total}(S) = L_{retr}(S) + \beta_{eff} \cdot L_{sec}(S). \quad (10)$$

The retrieval loss, $L_{retr}(S)$, is designed to quantify message recovery error in a manner compatible with our gradient-based optimization. While bit-level accuracy represents the ultimate performance metric, it is unsuitable for gradient-based optimization due to its discrete, non-differentiable nature. The L1 distance provides a continuous, differentiable surrogate that effectively approximates the integer recovery error. The mean L1 distance is therefore employed as a continuous and differentiable surrogate objective, calculated between the original message integers m and their estimates $\hat{m}(S)$:

$$L_{retr}(S) = \mathbb{E}[|m - \hat{m}(S)|_1]. \quad (11)$$

The security loss, L_{sec} , is designed to promote the statistical indistinguishability of the mapped noise $p(\mathbf{x}_T)$ from the SGD prior $\mathcal{N}(\mathbf{0}, \mathbf{I})$. We derive an analytical approximation of the Kullback-Leibler (KL) divergence $D_{KL}(p(\mathbf{x}_T) \parallel \mathcal{N}(\mathbf{0}, \mathbf{I}))$ based on the Gram-Charlier series expansion [42], and the complete derivation is provided in Appendix A:

$$D_{KL}(p(\mathbf{x}_T) \parallel \mathcal{N}(\mathbf{0}, \mathbf{I})) \approx \frac{1}{2} \sum_{j=2}^{\infty} \frac{(\kappa_{2j})^2}{(2j)!}. \quad (12)$$

This analytical formulation of D_{KL} provides a differentiable security loss term, and we define this term as $L_{sec} =$

$-1/\log(D_{KL})$ because this transformation creates a well-behaved loss landscape where minimizing the loss corresponds to minimizing the KL divergence.

The adaptive weighting mechanism adjusts β_{eff} based on current retrieval accuracy Acc_{curr} relative to a predefined target $Acc_{target}(Q)$. The adjustment follows a three-stage strategy:

- **Accuracy Deficit:** If $Acc_{curr} < Acc_{target}(Q) - \delta_1$, where δ_1 is a small margin, β_{eff} is significantly reduced. This strongly prioritizes the minimization of L_{retr} , forcing the optimizer to increase S to meet the minimum accuracy requirement.
- **Approaching Target:** If $Acc_{target}(Q) - \delta_1 \leq Acc_{curr} < Acc_{target}(Q)$, β_{eff} is moderately weighted. This allows for a more balanced optimization of both loss components as the system approaches the desired accuracy.
- **Target Achieved:** Once $Acc_{curr} \geq Acc_{target}(Q)$, β_{eff} is substantially increased. The focus now shifts to aggressively minimizing L_{sec} by reducing S as much as possible without falling below the accuracy target.

This state-dependent adaptation prioritizes message integrity requirements while seeking to optimize statistical security within practical constraints. The complete optimization procedure, performed offline for each capacity Q , is outlined in Algorithm 1.

V. EXPERIMENTS

This section details the empirical evaluation of our proposed steganography framework. Our primary objectives are threefold: first, to validate the proposed adaptive optimization protocol for the scale factor S ; second, to evaluate the framework’s performance in terms of embedding capacity, fidelity, and security across different architectures; and third, to conduct a systematic and comparative analysis of pixel-space versus VAE-based latent-space systems to investigate potential architecture dependent behaviors.

A. Experimental Protocol

All synthesis and inversion tasks employ the third-order DPM-Solver++ algorithm [37] with 50 sampling steps, utilizing publicly available pre-trained model weights, which remained frozen throughout our procedures. Experiments are conducted on an NVIDIA RTX 4090 GPU with PyTorch 2.7.0.

For pixel-space evaluation, we utilize pre-trained models for the LSUN Bedroom [43] and ImageNet [44] datasets, generating $3 \times 256 \times 256$ color images. In this configuration, an embedding rate factor of Q bits per component yields an effective embedding rate of Q bits per pixel per channel (bpp/ch). While latent-space evaluation is conducted through the Stable Diffusion v1.5 model [25], using prompts from the ImageInWords (IIW) dataset [45] as conditioning input. Since most LDM-based steganography methods use self-designed prompts, we recommend the IIW dataset as a standardized benchmark that enables fair evaluation and reproducible comparisons for future research. Data is embedded into the $4 \times 64 \times 64$ latent space, which is decoded to $3 \times 512 \times 512$ color images, yielding an effective embedding rate of $Q \cdot (4 \cdot 64 \cdot 64) / (3 \cdot 512 \cdot 512)$ bpp.

Performance assessment employs three established criteria. Image fidelity is quantified using the Fréchet Inception Distance (FID) [46], which measures the perceptual distance between generated and real image distributions. Message integrity is evaluated through the Bit Accuracy Rate (BAR) of extracted secret data. Security is assessed by training four widely-adopted deep learning-based steganalysis networks—SRNet [11], XuNet [12], YeNet [13], and SiaStegNet [14]—to distinguish stego images from a control set of non-steganography generations. The primary security metric is the minimum average classification error P_E , where values approaching the random-guess baseline of 0.5 indicate strongest security characteristics.

B. Validity of the Adaptive Optimization Framework

A key component of the methodology is the adaptive optimization protocol designed to determine an optimal scale S^* for each given embedding capacity Q . The effectiveness of this protocol depends on two conditions. The protocol must converge to a solution that balances a predefined retrieval accuracy target with security considerations. Additionally, the underlying security proxy must be valid. This section provides empirical evidence to evaluate both conditions.

The optimization was performed for capacities $Q \in \{1, 2, 4, 8\}$ across both pixel-space and latent-space architectures. The resultant optimal scale factors and key metrics at convergence are presented in Table I. The results reveal distinct, architecture dependent characteristics. For pixel-space models, the optimized S^* values are consistently small, reflecting the high numerical fidelity of the direct ODE inversion. The adaptive algorithm identifies values that meet the accuracy targets while maintaining correspondingly low KL divergence values D_{KL} . For the Latent Diffusion Model, substantially larger S^* values are required to achieve the accuracy targets. This reflects the information loss inherent in the VAE’s encode-decode cycle, necessitating greater initial separation of message levels in the latent space to ensure their preservation through the reconstruction process. The optimization protocol adapts to this requirement, converging to larger scale factors which result in higher latent-space D_{KL} values. These outcomes suggest that the adaptive procedure responds appropriately to the underlying properties of different generative model architectures.

TABLE I
OPTIMIZED SCALE FACTORS S^* AND ASSOCIATED METRICS FOR
PIXEL-SPACE AND LATENT DIFFUSION MODELS.

	Q	Acc_{target}	S^*	L_{retr}	D_{KL}
Bedroom	1	99.99%	0.0938	0.0326	1.93e-12
	2	99.00%	0.2111	0.0714	5.52e-11
	4	97.00%	0.5768	0.0310	2.63e-08
	8	95.00%	6.1440	0.3344	0.0582
ImageNet	1	99.99%	0.0992	0.0139	3.02e-12
	2	99.00%	0.1966	0.0682	3.13e-11
	4	97.00%	0.5413	0.1253	1.60e-08
	8	95.00%	5.6956	0.5073	0.0427
IIW	1	99.99%	2.7087	0.1361	0.1678
	2	98.00%	6.6104	0.2653	0.2891
	4	96.00%	12.3782	1.0486	0.3627
	8	90.00%	19.4804	16.6680	0.4388

A fundamental assumption of the optimization approach is the use of analytical KL divergence as a computationally efficient proxy for empirical security. To evaluate this assumption, a case study was conducted using the LSUN Bedroom dataset to examine the correlation between the scale factor S , the analytical D_{KL} , and the empirically measured security metric P_E against the panel of steganalysis networks. For this validation, seven different scale factor values were evaluated at a capacity of $Q = 4$ bpp/ch. For each scale factor evaluated, we generated a balanced dataset of 10,000 stego-cover image pairs, then the four steganalysis networks were trained to distinguish between them. The results are presented in Table II.

TABLE II
CORRELATION BETWEEN SCALE FACTOR S , ANALYTICAL D_{KL} ,
EMPIRICAL SECURITY P_E , AND RETRIEVAL ACCURACY BAR FOR $Q = 4$
ON BEDROOM DATASET.

Scale	D_{KL}	Empirical P_E				Acc (%)
		SRNet	XuNet	YeNet	SiaStegNet	
0.20	6.11e-12	0.495	0.494	0.498	0.496	89.71
0.40	1.50e-09	0.497	0.485	0.492	0.492	97.46
0.5768	2.63e-08	0.496	0.482	0.492	0.491	99.11
0.60	3.57e-08	0.496	0.482	0.488	0.490	99.27
0.80	3.23e-07	0.496	0.481	0.485	0.487	99.76
1.00	1.73e-06	0.495	0.480	0.480	0.487	99.90
1.50	2.98e-05	0.495	0.473	0.476	0.486	99.99

The results in Table II reveal a complex relationship between analytical KL divergence and empirical security performance. While XuNet, YeNet, and SiaStegNet demonstrate the expected inverse correlation between D_{KL} and detection error P_E , SRNet exhibits relatively stable performance across all scale factors, indicating potential insensitivity to the perturbations induced by this steganography method. Despite this limitation and the acknowledged gap between theoretical and estimated KL values at higher scale factors, the analytical KL divergence remains an effective and computationally efficient proxy for security assessment, as evidenced by consistent trends across three of the four evaluated networks. These findings support the continued use of KL divergence in the adaptive optimization framework while highlighting the importance of periodic empirical validation against diverse steganalysis architectures.

C. Analysis of Fidelity and Capacity

Visual examination of generated stego images is presented in Fig. (2). Across all three datasets, stego images at various embedding capacities appear visually indistinguishable from their non-steganography counterparts to human observers. The framework generates images without introducing conspicuous artifacts that would immediately reveal the presence of embedded secret information, thereby maintaining the imperceptibility necessary for covert communication applications.

Quantitative analysis, detailed in Table III, substantiates the qualitative visual findings and reveals key performance distinctions between architectures. For pixel-space models, the proposed framework demonstrates a compelling combination of high capacity and excellent fidelity. A key finding is that the FID score remains remarkably stable across a range of

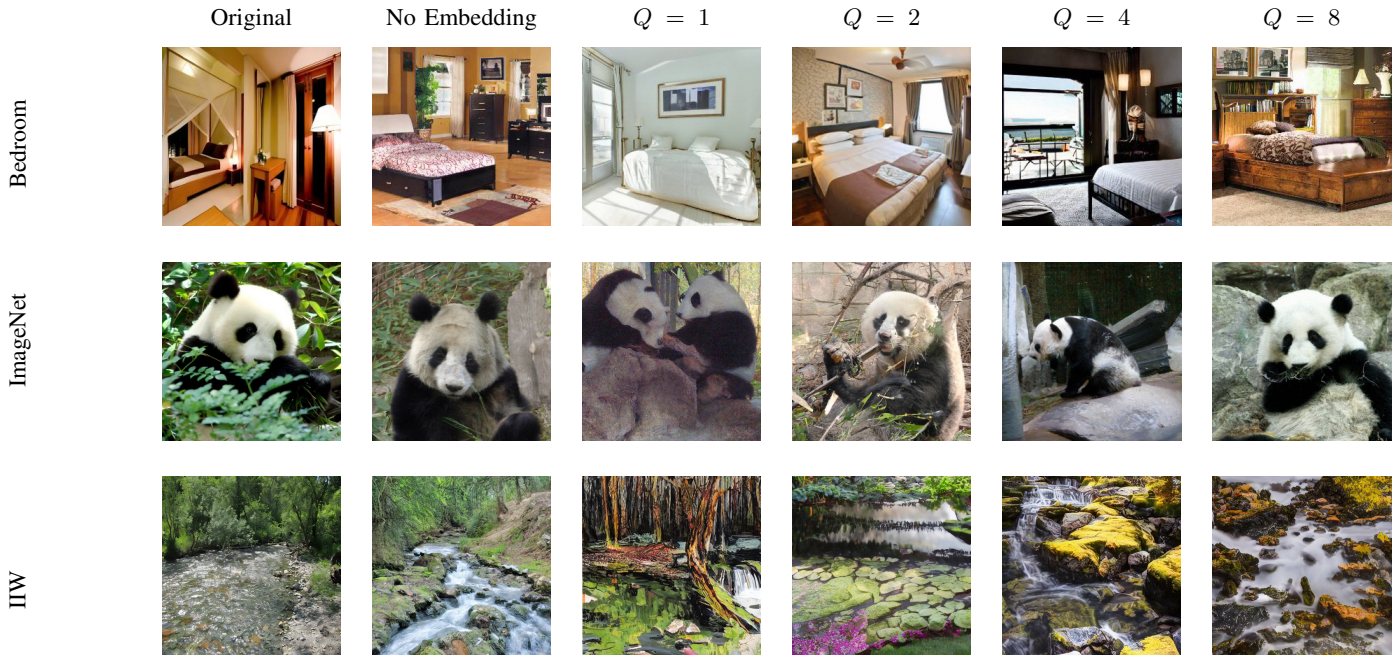


Fig. 2. Visual comparison of image fidelity across datasets and embedding capacities. Stego images generated with optimized S^* values maintain high visual similarity to their corresponding original and non-steganography counterparts, demonstrating effective imperceptibility.

TABLE III
COMPARATIVE ANALYSIS OF HIDING CAPACITY, FID, AND RETRIEVAL ACCURACY OF THE PROPOSED METHOD AND SOTA METHODS.

Method \ Metric	PROPOSED METHOD										SOTA METHODS									
	Bedroom (Pixel)					ImageNet (Pixel)					IIW (Latent)					Peng [19]	Zhou [21]	Hu [20]	Wei [32]	Su [33]
Capacity (bpp)	0	1	2	4	8	0	1	2	4	8	0	0.02	0.04	0.08	0.17	90.00	1.00	0.02	1.00	1.00
FID	3.68	3.70	3.69	3.68	4.17	18.86	19.05	19.10	18.64	17.91	52.04	57.71	59.34	60.09	61.16	-	11.38	16.60	13.21	5.59
BAR (%)	-	99.96	99.59	99.11	94.55	-	99.95	99.78	98.71	90.64	-	98.95	92.84	72.31	61.19	87.26	99.93	97.92	97.53	98.63

embedding rates, fluctuating around the baseline FID of the non-steganography generations for both the LSUN Bedroom and ImageNet datasets. This stability is attributable to the small, optimized scale factors selected by our adaptive protocol, which introduce only minimal perturbations to the generative process.

At the same embedding rates 1bpp for bedroom dataset, the proposed framework achieves superior fidelity and retrieval accuracy compared to both the diffusion-based method of Zhou et al. [21] and leading GAN-based systems by Wei et al. [32] and Su et al. [33].

In contrast, systems operating in a VAE-based latent space exhibit different characteristics. The use of a compressed latent representation inherently leads to lower effective embedding rates, a trait shared with other methods in this class, such as Hu et al. [20]. While visual quality is well-preserved, retrieval accuracy degrades more significantly at higher capacities. Targeted ablation analysis indicates that this information loss stems almost entirely from the VAE’s lossy encode-decode cycle rather than the diffusion process itself. Architectural differences also influence retrieval performance relative to GAN-based systems, the invertible ODE path of diffusion models generally affords higher accuracy than GANs, which

often rely on separately trained extractor networks.

For a comprehensive perspective, certain SOTA results are included for context. The exceptionally high capacities reported by Peng et al. [19] warrant a cautious interpretation due to methodological factors, including the use of an earlier DDPM sampler and a mapping process potentially sensitive to numeral error accumulation, a phenomenon empirically confirmed by Hu et al. [20]. Additionally, a separate class of image-in-image hiding research [38], [39] is acknowledged but not included in the direct quantitative comparison, as its evaluation centers on perceptual metrics for the recovered image rather than the retrieve accuracy used in this work.

D. Analysis of Security and Robustness

While the proposed framework demonstrates competitive performance on primary metrics, the comparative analysis across generative architectures reveals trade-off between security and robustness characteristics. This investigation indicates that this relationship extends beyond parametric optimization and appears to be a systemic property of the architectural choice between pixel-space and VAE-based latent-space systems.

TABLE IV
COMPARATIVE ANALYSIS OF STEGANALYSIS PERFORMANCE P_E ON THE PROPOSED METHOD AND SOTA WORKS.

Method Metric	PROPOSED METHOD												SOTA METHODS				
	Bedroom (Pixel)				ImageNet (Pixel)				IIW (Latent)				Zhou [21]	Peng [19]	Zhou [22]	Hu [20]	Wei [32]
Capacity (bpp)	1	2	4	8	1	2	4	8	0.02	0.04	0.08	0.17	1	-	1	0.02	1
SRNet [11]	0.491	0.489	0.490	0.342	0.496	0.494	0.494	0.485	0.089	0.063	0.062	0.050	-	0.490	-	0.508	0.479
XuNet [12]	0.494	0.493	0.494	0.331	0.495	0.496	0.495	0.350	0.431	0.425	0.421	0.418	-	-	0.270	0.502	-
YeNet [13]	0.488	0.479	0.479	0.478	0.497	0.491	0.487	0.487	0.260	0.251	0.239	0.208	0.496	0.500	-	0.479	-
SiaStegNet [14]	0.493	0.493	0.491	0.336	0.476	0.475	0.474	0.014	0.053	0.031	0.028	0.027	0.482	0.500	-	0.487	-

TABLE V
ROBUSTNESS OF THE PROPOSED METHODS UNDER VARIOUS ATTACKS. LDM DENOTES THE LATENT-SPACE MODEL ON IIW; PIXEL-SPACE DENOTES RESULTS ON BEDROOM / IMAGE.NET. ALL VALUES ARE PRESENTED IN PERCENTAGE FORM.

Method Attack	PROPOSED METHOD												SOTA METHODS			
	IIW (Latent)				Bedroom / ImageNet (Pixel)								Zhou [22]	Zhou [21]	Hu [20]	Su [33]
Capacity (bpp)	0.02	0.04	0.08	0.17	1	2	4	8	1	1	0.02	0.006	1	1	0.02	0.006
AWGN																
0.001	98.95	92.77	72.33	61.19	68.86 / 86.02	66.83 / 79.59	65.07 / 73.91	68.73 / 71.62	69	-	-	-	-	-	-	-
0.01	98.78	92.32	71.96	61.05	51.94 / 55.76	52.16 / 55.17	52.86 / 56.05	55.36 / 57.15	-	-	97	-	-	-	97	-
0.1	91.58	81.63	66.09	58.21	50.20 / 50.51	50.23 / 50.50	50.30 / 50.67	50.89 / 51.42	-	-	84	90	-	-	84	90
JPEG																
90	98.24	90.77	70.88	60.55	50.18 / 50.43	50.21 / 50.43	50.27 / 50.58	50.74 / 51.28	61	60	96	99	-	-	96	99
70	95.99	86.66	68.54	59.38	50.14 / 50.24	50.16 / 50.24	50.22 / 50.34	50.61 / 50.74	-	-	92	-	-	-	92	-
50	93.90	83.46	66.87	58.60	50.13 / 50.18	50.14 / 50.18	50.19 / 50.24	50.51 / 50.56	-	-	89	-	-	-	89	-
S&P																
1%	85.04	75.49	62.94	56.65	50.54 / 57.16	50.60 / 56.52	50.79 / 56.82	51.80 / 58.45	78	-	-	-	-	-	-	-
3%	80.10	70.39	60.49	55.43	50.30 / 52.73	50.34 / 52.66	50.46 / 53.24	51.15 / 54.26	73	-	-	-	-	-	-	-
5%	77.41	68.21	59.52	54.84	50.24 / 51.43	50.28 / 51.44	50.37 / 51.87	50.94 / 52.68	68	-	-	-	-	-	-	-
G-Blur																
3x3	97.64	89.36	70.07	60.14	50.72 / 50.97	50.80 / 50.95	51.08 / 51.29	52.25 / 52.74	-	-	97	99	-	-	97	99
5x5	93.59	82.16	66.20	58.27	50.23 / 50.27	50.25 / 50.27	50.34 / 50.36	50.81 / 50.92	-	-	96	-	-	-	96	-
7x7	87.61	75.00	62.84	56.60	50.10 / 50.13	50.11 / 50.13	50.15 / 50.18	50.38 / 50.45	-	-	93	-	-	-	93	-

a) *Security Analysis*: The security assessment through minimum average classification error P_E reveals distinct performance patterns across architectures, as detailed in Table IV. In pixel-space implementations at a capacity of 1 bpp, the framework maintains a exceeding 0.475 against a diverse panel of detectors. This result is comparable or superior to other high-performing diffusion-based methods [19], [21]. The framework also demonstrates a security advantage over other generative techniques, including position-based mapping [22] and certain GAN-based approaches [32].

In contrast to the pixel-space results, the VAE-based Stable Diffusion implementation exhibits a security vulnerability. As detailed in Table IV, modern detectors like SRNet and SiaStegNet identify the stego images with high accuracy, yielding detection error rates often approaching zero. While this contrasts with the higher security reported by Hu et al. [20], the disparity may be attributable to dataset differences; the detailed prompts in the IIW dataset can generate more complex images, providing a richer baseline for steganalysis. The varying effectiveness across steganalysis tools is also revealing, with performance correlating to their chronological development.

The high efficacy of recent models, contrasted with the insensitivity of older architectures like XuNet, indicates the VAE-based pipeline introduces a modern class of steganography traces. The systemic nature of this detectability suggests that standard latent diffusion architectures may inherently produce identifiable artifacts, implying that achieving robust security will likely require architectural innovation beyond parametric tuning.

b) *Robustness Analysis*: To assess the practical applicability of the framework, an evaluation of its robustness against common image processing attacks was conducted, with results presented as BAR in Table V. The findings reveal performance characteristics that are the inverse of the security results, highlighting a clear architecture-dependent relationship between security and robustness.

The pixel-space models, which exhibited high security, prove to be exceptionally fragile in lossy channels. Even minimal distortions, such as weak additive white Gaussian noise (AWGN), cause a substantial degradation in message retrieval accuracy. Stronger operations, including moderate JPEG compression, Gaussian blurring (G-Blur), or the introduction of sparse salt-

and-pepper (S&R) noise, lead to a complete collapse of message integrity, with the BAR approaching the 50% random-guess baseline. This fragility occurs because any perturbation to the stego image x_0 irrecoverably alters the trajectory of the sensitive ODE inversion process. This observation is consistent with related work on pixel-space diffusion steganography [21], reinforcing the view that such systems are primarily suited for lossless channels.

Conversely, the implementation on the VAE-based Stable Diffusion system demonstrates a high degree of robustness against a wide range of distortions. For example, at an embedding rate of 0.02 bpp, the system maintains over 93% BAR against aggressive JPEG-50 compression and still achieves over 85% BAR even when 1% of pixels are corrupted by S&R noise. This performance is highly competitive with other SOTA methods, including the LDM-based approach of Hu et al. [20] and the robust GAN-based system by Su et al. [33]. This observed resilience is closely linked to the VAE component of the architecture. A detailed mechanistic analysis of how the VAE's encoder contributes to this robustness is presented in Section V-E.

c) Synthesis of Findings: The combined results from the security and robustness evaluations provide strong evidence for an architecture-dependent relationship between these two critical properties in diffusion-based steganography. The analysis indicates that pixel-space models can offer a path toward high security, but this comes at the cost of extreme fragility in lossy channels. In contrast, VAE-based latent-space systems provide substantial robustness but appear to introduce systemic security vulnerabilities. This suggests that no single, standard architecture examined in this work simultaneously satisfies the core requirements for a universally practical, secure, and robust steganography system. This finding may reframe a central challenge in the field, suggesting that progress could depend as much on architectural innovation as on the parametric optimization of specific embedding methods. Future research could therefore focus on developing novel frameworks capable of resolving these conflicting performance characteristics.

E. Analysis of the VAE's Role in Security and Robustness

The preceding analysis established a relationship between the generative architecture and the resulting security and robustness performance. This section presents a targeted investigation into the VAE component of the Stable Diffusion system, examining the hypothesis that it is the main mechanism behind this observed relationship. The analysis explores the distinct functional roles of the VAE's encoder and decoder, providing evidence that they contribute to robustness and security vulnerabilities respectively.

a) The Decoder as an Artifact Amplifier: To isolate the source of security vulnerabilities in VAE-based systems, a multi-faceted statistical analysis of steganography residuals was conducted. The steganography residual is defined as the absolute difference between a steganography output and a corresponding clean baseline, averaged over thousands of samples to reveal systematic patterns. This residual is compared against a control residual, which is generated by replacing the

steganography signal with an energy-matched random noise signal. The control provides a baseline for the system's natural statistical variations, allowing for a precise assessment of the artifacts introduced by the steganography process itself, as shown in Fig. (3).

The pixel-space model exhibits high statistical similarity between steganography and control residuals, with histogram distributions showing near-perfect overlap as shown in Fig. (3a). In contrast, the VAE-based system reveals a systematic vulnerability through a two-stage amplification process. The latent-space analysis shows that the U-Net generates a subtle artifact, evidenced by a rightward shift in the steganography residual histogram compared to the control group in Fig. (3b), and the VAE decoder subsequently amplifies this subtle latent-space deviation, transforming it into a pronounced distributional shift in the pixel-space residual histogram shown in Fig. (3c).

Spectral analysis provides additional evidence for this amplification mechanism. The pixel-space model exhibits nearly identical DC components and spectral profiles between steganography and control residuals, shown as Fig. (3d), indicating minimal artifact generation. In contrast, the latent-space analysis reveals that steganography residuals exhibit elevated DC components compared to control residuals, as observed in Fig. (3e). The VAE decoder systematically transforms these subtle latent-space deviations into pronounced pixel-space artifacts, amplifying the low-frequency disparity and introducing sharp high-frequency spectral spikes in the final pixel-space residual shown in Fig. (3f).

b) The Encoder as a Manifold Regularizer: To explain the pronounced robustness of the LDM system, the behavior of the VAE encoder when processing corrupted steganography images was investigated. The hypothesis examined posits that the encoder confers robustness by regularizing attacked image representations toward the learned manifold of valid image latents, effectively functioning as a denoising mechanism. This hypothesis was tested by measuring how attacks simultaneously affect message retrieval accuracy and the distance between latent vectors and the geometric center of the true data manifold.

Analysis under varying levels of AWGN serves as a case study to reveal core mechanisms, with results presented in Fig. (4). A manifold regularization effect is clearly observable under weak noise with a standard deviation of 0.001. For this condition 61.44% of attacked samples are projected closer to the manifold's center by the VAE encoder than their unattacked counterparts. This demonstrates the encoder's strong generative prior and its tendency to map perturbed inputs toward high-density regions of the latent space. However, this regularization capability exhibits clear limitations. As the noise intensity increases, the effect progressively diminishes and eventually fails. Under strong noise conditions, the encoder's regularization mechanism becomes ineffective, with nearly all samples being pushed further from the manifold center. This indicates that while the encoder's capacity to map corrupted, off-manifold pixel data back onto the constrained latent space can sanitize inputs for the reverse ODE solver under mild distortions, this ability is fundamentally limited and does not confer robustness against severe channel noise.

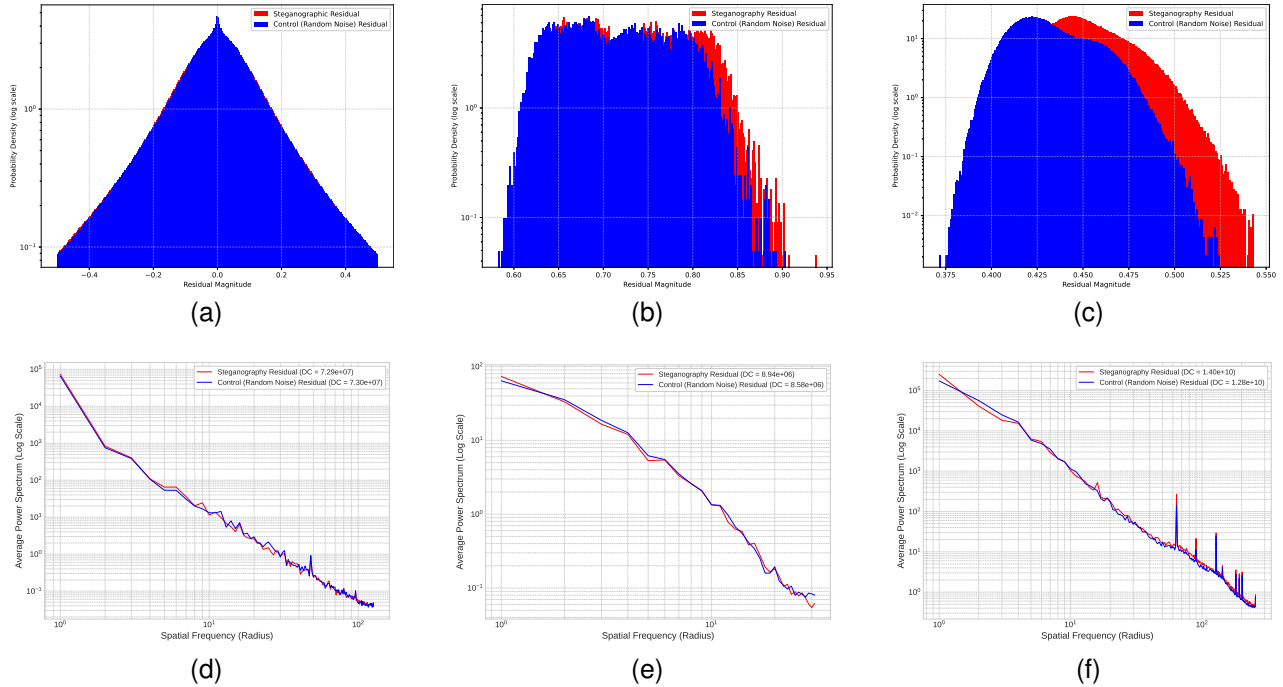


Fig. 3. Comparative analysis of steganography residuals. Top row (a-c): histograms; bottom row (d-f): radially averaged power spectra. (a,d) Pixel-space model shows high similarity between steganography and control conditions. (b,e) Latent-space analysis reveals subtle U-Net-induced deviations with modest low-frequency elevation. (c,f) VAE decoder amplifies these into pronounced pixel-space distributional shifts and spectral artifacts with low-frequency amplification and high-frequency spikes.

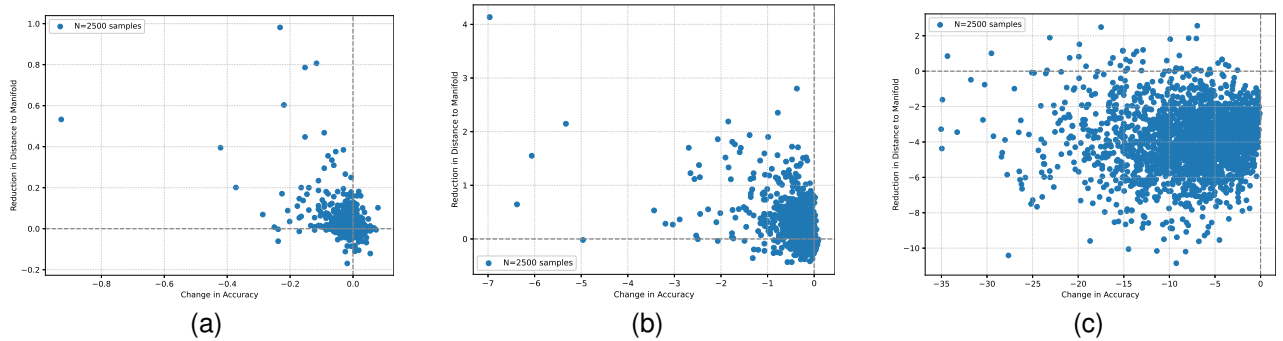


Fig. 4. Correlation between latent manifold distance reduction and retrieval accuracy changes under AWGN attacks at $Q = 1$. (a) Weak noise ($\sigma = 0.001$): 61.44% of samples show manifold regularization (positive Y-axis) without consistent accuracy improvement (negative X-axis). (b) Moderate noise ($\sigma = 0.01$): regularization effect diminishes. (c) Strong noise ($\sigma = 0.1$): regularization vanishes, samples are pushed from manifold causing accuracy degradation.

VI. CONCLUSION

This work presented a systematic investigation into the relationship between security and robustness in diffusion-based steganography, enabled by a novel and computationally efficient framework based on an adaptively optimized approximate Gaussian mapping. The analysis provides evidence for an architecture dependent performance trade-off, where pixel-space diffusion models can achieve high security at the cost of fragility, while VAE-based systems offer substantial robustness but introduce systemic security vulnerabilities. A mechanistic analysis of the VAE component suggests a dual functionality, with its encoder conferring robustness through manifold regularization and its decoder introducing detectable artifacts by amplifying latent perturbations.

The findings indicate that a central challenge in generative

steganography extends beyond the optimization of embedding parameters to the core architectural design. The conflicting performance characteristics identified in this study suggest that achieving a system that is simultaneously secure, robust, and high capacity may require architectural innovations. Promising directions for future research include the co-design of embedding strategies with the generative process itself and the development of architectures that mitigate the VAE’s dual-natured impact on steganography performance.

APPENDIX

This appendix presents a detailed derivation of the analytical approximation for the KL divergence between the distribution of the mapped noise variable \mathbf{x}_T and a standard normal distribution $\mathcal{N}(\mathbf{0}, \mathbf{I})$. This approximation serves as the computationally

efficient security proxy L_{sec} within the adaptive optimization framework.

The objective is to compute $D_{KL}(p(\mathbf{x}_T)||\phi)$, where $p(\mathbf{x}_T)$ represents the probability density function of the mapped noise and $\phi(x)$ denotes the PDF of $\mathcal{N}(\mathbf{0}, \mathbf{I})$. The variable \mathbf{x}_T is defined as:

$$\mathbf{x}_T = \frac{u+n}{\sigma}, \quad u = S \cdot \left(\frac{m}{2^Q - 1} - 0.5 \right), \quad n \sim \mathcal{N}(\mathbf{0}, \mathbf{I}). \quad (\text{A1})$$

The message component m follows a discrete uniform distribution over $\{0, 1, \dots, N-1\}$, where $N = 2^Q$. The normalization factor $\sigma = \sqrt{1 + \text{Var}(u)}$ ensures that $\text{Var}(\mathbf{x}_T) = 1$.

The derivation utilizes the relationship between distributional moments and cumulants, employing a Gram-Charlier Type A series to approximate the PDF. The required central moments of the discrete uniform distribution for m are:

$$\begin{aligned} \mu_2(m) &= \frac{N^2 - 1}{12} \\ \mu_4(m) &= \frac{(N^2 - 1)(3N^2 - 7)}{240} \\ \mu_6(m) &= \frac{(N^2 - 1)(3N^4 - 18N^2 + 31)}{1344} \\ \mu_8(m) &= \frac{(N^2 - 1)(5N^6 - 55N^4 + 239N^2 - 381)}{11520} \\ \mu_{10}(m) &= \frac{(N^2 - 1)(5N^8 - 80N^6 + 580N^4 - 2488N^2 + 4931)}{24024} \end{aligned} \quad (\text{A2})$$

The procedure involves computing the cumulants of the unnormalized variable $X = u + n$, then scaling them to determine the cumulants of $\mathbf{x}_T = X/\sigma$.

The symmetric construction of variable u centered at zero and the inherent symmetry of the Gaussian noise n ensure that their sum X maintains symmetry. Consequently, all odd-order central moments and cumulants of X and \mathbf{x}_T equal zero:

$$\kappa_{2k-1}(\mathbf{x}_T) = 0, \quad \forall k \geq 1. \quad (\text{A3})$$

By construction, the initial two cumulants are $\kappa_1(\mathbf{x}_T) = E[\mathbf{x}_T] = 0$ and $\kappa_2(\mathbf{x}_T) = \text{Var}(\mathbf{x}_T) = 1$. The even-order cumulants $\kappa_{2j}(\mathbf{x}_T)$ for $j \geq 2$ are derived using the additivity property of cumulants for independent random variables: $\kappa_r(u+n) = \kappa_r(u) + \kappa_r(n)$. Since n follows a Gaussian distribution, its cumulants $\kappa_r(n)$ equal zero for all $r \geq 3$. Therefore, $\kappa_r(X) = \kappa_r(u)$ for $r \geq 3$. The cumulants of \mathbf{x}_T follow the scaling property: $\kappa_r(X/\sigma) = \kappa_r(X)/\sigma^r$.

This reduces the problem to determining the cumulants of u . The r -th cumulant $\kappa_r(u)$ represents a polynomial of the central moments of u up to order r . The central moments of u relate directly to the central moments of m :

$$\mu_r(u) = E[u^r] = \frac{S^r}{(N-1)^r} \mu_r(m). \quad (\text{A4})$$

By expressing the cumulants in terms of moments, the closed-form expressions for the cumulants of \mathbf{x}_T can be derived. The

initial four non-zero higher-order cumulants are:

$$\begin{aligned} \kappa_4(\mathbf{x}_T) &= -\frac{6S^4(N+1)(N^2+1)}{5(N-1)(12(N-1)+S^2(N+1))^2} \\ \kappa_6(\mathbf{x}_T) &= \frac{48S^6(N^6-1)}{7(N-1)^3(12(N-1)+S^2(N+1))^3} \\ \kappa_8(\mathbf{x}_T) &= -\frac{4320S^8(N^8-1)}{11(N-1)^4(12(N-1)+S^2(N+1))^4} \\ \kappa_{10}(\mathbf{x}_T) &= \frac{207360S^{10}(N^{10}-1)}{13(N-1)^5(12(N-1)+S^2(N+1))^5} \end{aligned} \quad (\text{A5})$$

The Gram-Charlier Type A series approximates the PDF $p(\mathbf{x}_T)$ using its cumulants and the probabilists' Hermite polynomials $H_r(x)$:

$$\begin{aligned} p(\mathbf{x}_T) &\approx \phi(x) \left[1 + \sum_{j=2}^k \frac{\kappa_{2j}}{(2j)!} H_{2j}(x) \right] \\ &= \phi(x) [1 + \mathcal{H}(x)]. \end{aligned} \quad (\text{A6})$$

The truncation extends to the 10th cumulant. The KL divergence is defined as $D_{KL} = \int p(\mathbf{x}_T) \log(p(\mathbf{x}_T)/\phi(x)) dx$. Substituting the series expansion yields:

$$D_{KL} \approx \int \phi(x) [1 + \mathcal{H}(x)] \log[1 + \mathcal{H}(x)] dx. \quad (\text{A7})$$

For steganographic applications, S typically remains small, ensuring that the cumulants κ_{2j} are small and thus $|\mathcal{H}(x)| \ll 1$. This allows employment of a Taylor series expansion for the logarithm, $\log(1+y) \approx y - y^2/2$:

$$\begin{aligned} D_{KL} &\approx \int \phi(x) [1 + \mathcal{H}(x)] \left(\mathcal{H}(x) - \frac{\mathcal{H}(x)^2}{2} \right) dx \\ &\approx \int \phi(x) \left(\mathcal{H}(x) + \frac{\mathcal{H}(x)^2}{2} \right) dx. \end{aligned} \quad (\text{A8})$$

The probabilists' Hermite polynomials exhibit orthogonality with respect to the Gaussian weighting function $\phi(x)$, with $\int H_r(x)\phi(x)dx = 0$ for $r \geq 1$. This eliminates the initial term, $\int \mathcal{H}(x)\phi(x)dx = 0$. The orthogonality property, $\int H_r(x)H_s(x)\phi(x)dx = r!\delta_{rs}$, simplifies the second term:

$$\begin{aligned} \int \phi(x) \frac{\mathcal{H}(x)^2}{2} dx &= \frac{1}{2} \int \phi(x) \left(\sum_{j=2}^k \frac{\kappa_{2j}}{(2j)!} H_{2j}(x) \right)^2 dx \\ &= \frac{1}{2} \sum_{j=2}^k \frac{(\kappa_{2j})^2}{(2j)!}. \end{aligned} \quad (\text{A9})$$

This yields the analytical approximation for the KL divergence:

$$D_{KL}(p(\mathbf{x}_T)||\phi(x)) \approx \frac{1}{2} \left(\frac{\kappa_4^2}{4!} + \frac{\kappa_6^2}{6!} + \frac{\kappa_8^2}{8!} + \frac{\kappa_{10}^2}{10!} \right). \quad (\text{A10})$$

The derivation relies on two key approximations: the truncation of the Gram-Charlier series and the Taylor expansion of the logarithm. The validity of both approximations is highest when the distribution $p(\mathbf{x}_T)$ represents only a small perturbation from the standard Gaussian, corresponding to scenarios with small scale factors S . Consequently, while this analytical formula

provides a computationally efficient and differentiable proxy for security, its quantitative accuracy diminishes as S increases. For the large S^* values necessitated by high-capacity embedding, particularly in the LDM framework, the computed D_{KL} values should be interpreted primarily as qualitative indicators of statistical deviation rather than precise information-theoretic measurements.

REFERENCES

- [1] J. Ho, A. Jain, and P. Abbeel, "Denosing diffusion probabilistic models," in *Proc. Adv. Neural Inf. Process. Syst.*, vol. 33, 2020, pp. 6840–6851.
- [2] I. Goodfellow et al., "Generative adversarial nets," in *Proc. Adv. Neural Inf. Process. Syst.*, Montréal, QC, Canada, 2014, pp. 2672–2680.
- [3] D. P. Kingma and P. Dhariwal, "Glow: Generative flow with invertible 1x1 convolutions," in *Proc. Adv. Neural Inf. Process. Syst.*, 2018, pp. 10236–10245.
- [4] J. Fridrich, "Steganography in digital media: Principles, algorithms, and applications," *IEEE Signal Process. Mag.*, vol. 28, no. 5, pp. 142–144, Apr. 2011.
- [5] C.-K. Chan and L. M. Cheng, "Hiding data in images by simple LSB substitution," *Pattern Recognit.*, vol. 37, no. 3, pp. 469–474, Mar. 2004.
- [6] T. Pevn'y, T. Filler, and P. Bas, "Using high-dimensional image models to perform highly undetectable steganography," in *Proc. 12th Int. Conf. Inf. Hiding (IH)*, Calgary, AB, Canada, 2010, pp. 161–177.
- [7] V. Holub, J. Fridrich, and T. Denemark, "Universal distortion function for steganography in an arbitrary domain," *EURASIP J. Inf. Secur.*, vol. 2014, pp. 1–13, Jan. 2014.
- [8] B. Li, M. Wang, and J. Huang, "A new cost function for spatial image steganography," in *Proc. IEEE Int. Conf. Image Process. (ICIP)*, Paris, France, Oct. 2014, pp. 4206–4210.
- [9] V. Holub and J. Fridrich, "Designing steganography distortion using directional filters," in *Proc. 4th IEEE Int. Workshop Inf. Forensics Secur.*, Tenerife, Spain, Dec. 2012, pp. 234–239.
- [10] T. Filler, J. Judas, and J. Fridrich, "Minimizing additive distortion in steganography using syndrome-trellis codes," *IEEE Trans. Inf. Forensics Security*, vol. 6, no. 3, pp. 920–935, Sep. 2011.
- [11] M. Boroumand, M. Chen, and J. Fridrich, "Deep residual network for steganalysis of digital images," *IEEE Trans. Inf. Forensics Security*, vol. 14, no. 5, pp. 1181–1193, May 2019.
- [12] G. Xu, H.-Z. Wu, and Y.-Q. Shi, "Structural design of convolutional neural networks for steganalysis," *IEEE Signal Process. Lett.*, vol. 23, no. 5, pp. 708–712, May 2016.
- [13] J. Ye, J. Ni, and Y. Yi, "Deep learning hierarchical representations for image steganalysis," *IEEE Trans. Inf. Forensics Security*, vol. 12, no. 11, pp. 2545–2557, Nov. 2017.
- [14] W. You, H. Zhang, and X. Zhao, "A Siamese CNN for image steganalysis," *IEEE Trans. Inf. Forensics Security*, vol. 16, pp. 291–306, 2021.
- [15] Z. Zhou, H. Sun, R. Harit, X. Chen, and X. Sun, "Coverless image steganography without embedding," in *Proc. 1st Int. Conf. Cloud Comput. Secur. (ICCCS)*, Nanjing, China, 2015, pp. 123–132.
- [16] Q. Liu, X. Xiang, J. Qin, Y. Tan, J. Tan, and Y. Luo, "Coverless steganography based on image retrieval of DenseNet features and DWT sequence mapping," *Knowl.-Based Syst.*, vol. 192, Mar. 2020, Art. no. 105342.
- [17] Y. Luo, J. Qin, X. Xiang, and Y. Tan, "Coverless image steganography based on multi-object recognition," *IEEE Trans. Circuits Syst. Video Technol.*, vol. 31, no. 7, pp. 2779–2791, Jul. 2021.
- [18] X. Liu, Z. Li, J. Ma, W. Zhang, J. Zhang, and Y. Ding, "Robust coverless steganography using limited mapping images," *J. King Saud Univ.-Comput. Inf. Sci.*, vol. 34, no. 7, pp. 4472–4482, May 2022.
- [19] Y. Peng, D. Hu, Y. Wang, K. Chen, G. Pei, and W. Zhang, "Stegaddpm: Generative image steganography based on denoising diffusion probabilistic model," in *Proc. 31st ACM Int. Conf. Multimedia*, 2023, pp. 7143–7151.
- [20] X. Hu, S. Li, Q. Ying, W. Peng, X. Zhang, and Z. Qian, "Establishing robust generative image steganography via popular stable diffusion," *IEEE Trans. Inf. Forensics Security*, vol. 19, pp. 8094–8108, 2024.
- [21] Q. Zhou, P. Wei, Z. Qian, X. Zhang, and S. Li, "Improved generative steganography based on diffusion model," *IEEE Trans. Circuits Syst. Video Technol.*, 2025. [Online]. Available: DOI: 10.1109/TCSVT.2025.3539832.
- [22] Z. Zhou, "Secret-to-image reversible transformation for generative steganography," *IEEE Trans. Depend. Secure Comput.*, vol. 20, no. 5, pp. 4118–4134, Sep./Oct. 2023.
- [23] D. P. Kingma and M. Welling, "Auto-encoding variational Bayes," 2013, *arXiv:1312.6114*.
- [24] R. Rombach, A. Blattmann, D. Lorenz, P. Esser, and B. Ommer, "High-resolution image synthesis with latent diffusion models," in *Proc. IEEE/CVF Conf. Comput. Vis. Pattern Recognit.*, 2022, pp. 10684–10695.
- [25] R. Rombach, A. Blattmann, D. Lorenz, P. Esser, and B. Ommer, "High-resolution image synthesis with latent diffusion models," in *Proc. IEEE/CVF Conf. Comput. Vis. Pattern Recognit.*, Jun. 2022, pp. 10684–10695.
- [26] J. Mielikainen, "LSB matching revisited," *IEEE Signal Process. Lett.*, vol. 13, no. 5, pp. 285–287, May 2006.
- [27] A. Westfeld and A. Pfitzmann, "Attacks on steganography systems: Breaking the steganography utilities EzStego, Jsteg, Steganos, and S-Tools-and some lessons learned," in *Proc. Int. Workshop Inf. Hiding*, 1999, pp. 61–75.
- [28] D. Volkhonskiy, I. Nazarov, and E. Burnaev, "steganography generative adversarial networks," in *Proc. 12th Int. Conf. Mach. Vis.*, 2020, Art. no. 114333M.
- [29] H. Shi, J. Dong, W. Wang, Y. Qian, and X. Zhang, "SSGAN: Secure steganography based on generative adversarial networks," in *Proc. Pacific Rim Conf. Multimedia*, 2017, pp. 534–544.
- [30] Z. Zhang, G. Fu, R. Ni, J. Liu, and X. Yang, "A generative method for steganography by cover synthesis with auxiliary semantics," *Tsinghua Sci. Technol.*, vol. 25, no. 4, pp. 516–527, 2020.
- [31] X. Liu, Z. Ma, J. Ma, J. Zhang, G. Schaefer, and H. Fang, "Image disentanglement autoencoder for steganography without embedding," in *Proc. IEEE/CVF Conf. Comput. Vis. Pattern Recognit.*, 2022, pp. 2303–2312.
- [32] P. Wei, S. Li, X. Zhang, G. Luo, Z. Qian, and Q. Zhou, "Generative steganography network," in *Proc. 30th ACM Int. Conf. Multimedia*, 2022, pp. 1621–1629.
- [33] W. Su, J. Ni, and Y. Sun, "Stegastylegan: Towards generic and practical generative image steganography," in *Proc. AAAI Conf. Artif. Intell.*, vol. 38, no. 1, 2024, pp. 240–248.
- [34] D. Hu, L. Wang, W. Jiang, S. Zheng, and B. Li, "A novel image steganography method via deep convolutional generative adversarial networks," *IEEE Access*, vol. 6, pp. 38303–38314, 2018.
- [35] Y. Song, J. Sohl-Dickstein, D. P. Kingma, A. Kumar, S. Ermon, and B. Poole, "Score-based generative modeling through stochastic differential equations," in *Proc. 9th Int. Conf. Learn. Represent. (ICLR)*, Vienna, Austria, May 2021, pp. 1–36.
- [36] C. Lu, Y. Zhou, F. Bao, J. Chen, C. Li, and J. Zhu, "DPM-solver: A fast ODE solver for diffusion probabilistic model sampling in around 10 steps," in *Proc. Adv. Neural Inf. Process. Syst.*, vol. 35, 2022, pp. 5775–5787.
- [37] C. Lu, Y. Zhou, F. Bao, J. Chen, C. Li, and J. Zhu, "DPM-Solver++: Fast solver for guided sampling of diffusion probabilistic models," 2022, *arXiv:2211.01095*.
- [38] J. Yu, X. Zhang, Y. Xu, and J. Zhang, "Cross: Diffusion model makes controllable, robust and secure image steganography," *Adv. Neural Inf. Process. Syst.*, vol. 36, 2024.
- [39] L. Chen, B. Feng, Z. Xia, W. Lu, and J. Weng, "Robust generative steganography for image hiding using concatenated mappings," *IEEE Trans. Inf. Forensics Security*, 2025. [Online]. Available: DOI: 10.1109/TIFS.2025.3573669.
- [40] J. Song, C. Meng, and S. Ermon, "Denoising diffusion implicit models," in *Proc. 9th Int. Conf. Learn. Represent. (ICLR)*, Vienna, Austria, May 2021, pp. 1–22.
- [41] J. Daemen and V. Rijmen, *The Design of Rijndael*, vol. 2. Berlin, Germany: Springer, 2002.
- [42] A. Hald, "The early history of the cumulants and the Gram-Charlier series," *Int. Stat. Rev.*, vol. 68, no. 2, pp. 137–153, Aug. 2000.
- [43] F. Yu, A. Seff, Y. Zhang, S. Song, T. Funkhouser, and J. Xiao, "Lsun: Construction of a large-scale image dataset using deep learning with humans in the loop," 2015, *arXiv:1506.03365*.
- [44] J. Deng, W. Dong, R. Socher, L. Li, K. Li, and F. Li, "ImageNet: A large-scale hierarchical image database," in *Proc. IEEE Conf. Comput. Vis. Pattern Recognit.*, 2009, pp. 248–255.
- [45] R. Garg, A. Burns, B. Karagol Ayan, Y. Bitton, C. Montgomery, Y. Onoe, A. Bunner, R. Krishna, J. Baldrige, and R. Soricut, "ImageInWords: Unlocking hyper-detailed image descriptions," 2024, *arXiv:2405.02793*.
- [46] M. Heusel, H. Ramsauer, T. Unterthiner, B. Nessler, and S. Hochreiter, "GANs trained by a two time-scale update rule converge to a local Nash equilibrium," in *Proc. Adv. Neural Inf. Process. Syst.*, vol. 30, 2017, pp. 1–12.